iScience

CellPress
OPEN ACCESS

Article

Uncovering lipopolysaccharide regulation in bacteria via the critical lipid binding tunnel of YciS/YciM

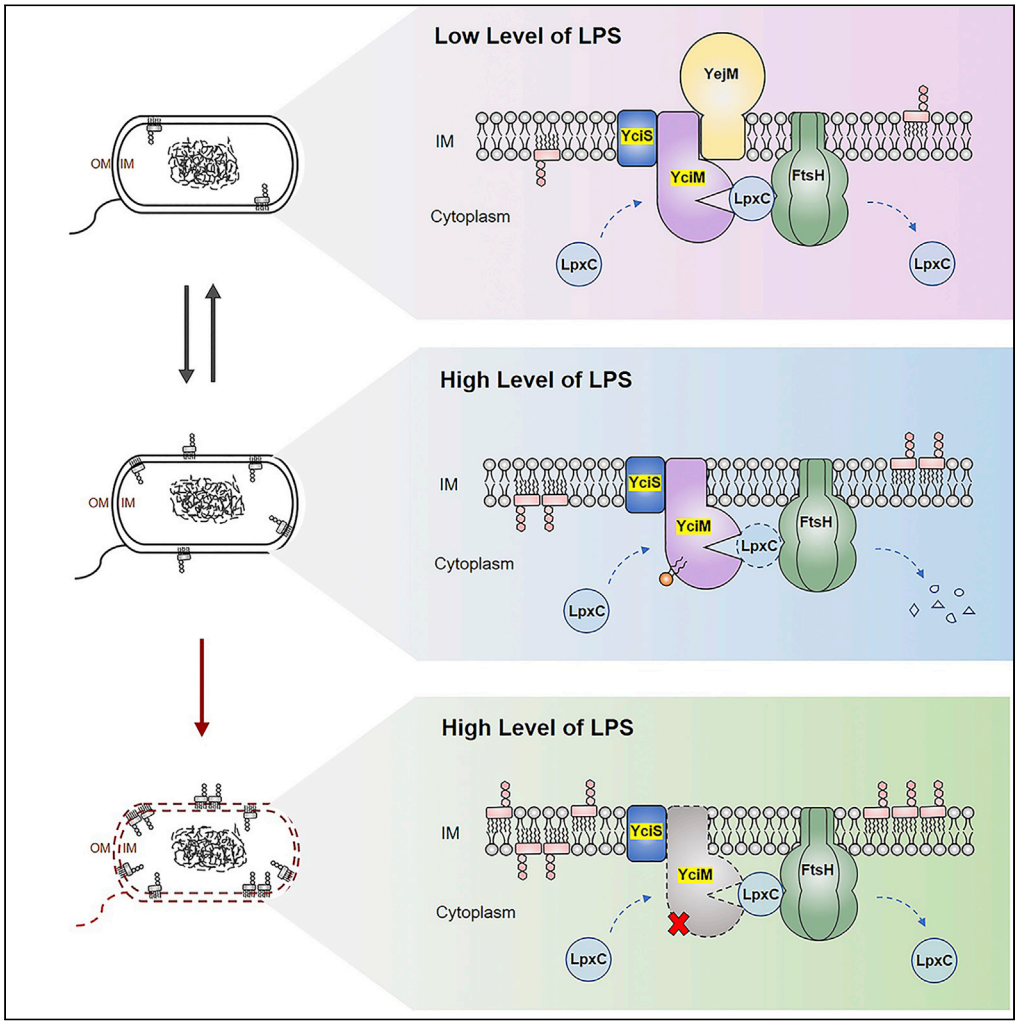

Lina Yan, Haohao Dong, Huanyu Li, Xingyu Liu, Zixin Deng, Changjiang Dong, Zhengyu Zhang

zhengyu.zhang@whu.edu.cn

Highlights

Identifying a critical lipid binding tunnel of YciS/YciM

The lipid binding tunnel could bind lipid molecules

Mutants of lipid binding tunnel inhibit cell growth severely

Yan et al., iScience 25, 104988
September 16, 2022
https://doi.org/10.1016/j.isci.2022.104988

iScience

CellPress
OPEN ACCESS

Article

Uncovering lipopolysaccharide regulation in bacteria via the critical lipid binding tunnel of YciS/YciM

Lina Yan,[1,2] Haohao Dong,[3] Huanyu Li,[4] Xingyu Liu,[5] Zixin Deng,[1,2] Changjiang Dong,[1,2] and Zhengyu Zhang[1,2,6,*]

SUMMARY

Gram-negative bacteria contain an asymmetric outer membrane, in which the outer leaflet is composed of lipopolysaccharide (LPS). LPS, a drug target of polymyxin, plays an essential role in drug resistance, biofilm formation, and pathogenesis. An important inner membrane protein, YciM, may be responsible for the regulation of LPS biosynthesis and transport. Here, we report the crystal structure of YciM from *Salmonella typhimurium* in a complex with a non-specifically bond molecule, an ethylene glycol, which identified a tunnel that could bind lipids. Our *in vitro* assays showed that YciM could bind lipid molecules with affinity in the micromolar range, while mutagenic and functional studies confirmed that lipid-binding residues are critical for the function of YciM. Additionally, our data also showed that YciM accurately regulates LPS biosynthesis and transport with YciS, which could help to better understand the regulation mechanism of LPS.

INTRODUCTION

The cell envelope of Gram-negative bacteria contains three distinct structures, the inner membrane (IM), the periplasm, and the outer membrane (OM). The OM is an asymmetric lipid bilayer, of which the outer leaflet consists of LPS. The deficiency or impairment of LPS would lead to loss of membrane integrity and cell death for most Gram-negative bacteria (Wang and Quinn, 2010). Lipid A, a prominent component of LPS, has high heterogeneity that is controlled by diverse regulatory factors and growth conditions (Klein et al., 2011). Bacteria maintain OM lipid asymmetry and stability to protect themselves from the intrusion of toxic substances, such as antibiotics, detergents, and dyes (Konovalova et al., 2017; Moffatt et al., 2019).

The function of OM was mainly maintained by its lipid asymmetry; the perturbation of lipid asymmetry would cause elevated cell membrane permeability and toxic substances easily invading (Henderson et al., 2016). The broken balance between LPS and phospholipids is the major factor that caused perturbation of lipid asymmetry, and the biosynthetic pathway of LPS and phospholipids has been well characterized in *E. coli* (*Escherichia coli*) (Wang et al., 2015). The Kdo_2-lipid A biosynthetic pathway begins with the building block, N-acetyl glucosamine linked to the nucleotide carrier. LpxA catalyzes the first reaction; it transfers an R-3-hydroxyacyl chain to the N-acetyl glucosamine (Williams and Raetz, 2007). R-3-hydroxyacyl-ACP is also the substrate of FabZ in the phospholipid biosynthetic pathway (Zhang et al., 2016). It has been suggested to be a key factor in maintaining the dynamic equilibrium between LPS and phospholipids (Emiola et al., 2016; Heath and Rock, 1996; Williams and Raetz, 2007). As the equilibrium constant for the first reaction catalyzed by LpxA is unfavorable, LpxC performs the first committed step of lipid A biogenesis, which strictly regulates the level of LPS, and is imperative for cell growth (Barb and Zhou, 2008). Some studies have shown that LpxC is a validated target for the development of effective inhibitors and the design of novel antibiotics (Barb et al., 2007; Jackman et al., 2000; Piizzi et al., 2017; Tomaras et al., 2014).

It has been reported that the level of LpxC is affected by the AAA + protease protein FtsH (Fivenson and Bernhardt, 2020). The unstructured C-terminal of LpxC containing the motif LAXXXXXAVLA could be recognized and degraded by FtsH. This special structure is indispensable in helping LpxC through the pore of FtsH but is not sufficient for LpxC to be degraded by FtsH (Fuhrer et al., 2007). The absence of FtsH leads to a rise in LpxC expression and an accumulation of LPS that causes cell death. Moreover, according to the studies in 2014, YciM is necessary for FtsH to regulate LPS biogenesis in *E. coli* (Klein et al.,

[1]School of Pharmaceutical Sciences, Wuhan University, Wuhan 430071, China

[2]Key Laboratory of Combinatorial Biosynthesis and Drug Discovery, Ministry of Education, Wuhan University School of Pharmaceutical Sciences, 430071 Wuhan, China

[3]State Key Laboratory of Biotherapy and Cancer Center, National Clinical Research Center for Geriatrics, West China Hospital, Sichuan University and Collaborative Innovation Center of Biotherapy, Chengdu, Sichuan, China

[4]Structural Genomics Consortium, University of Oxford, Oxford

[5]College of chemistry and molecular sciences, Wuhan University, Wuhan, Hubei, China

[6]Lead contact

*Correspondence: zhengyu.zhang@whu.edu.cn

https://doi.org/10.1016/j.isci.2022.104988

2014). The amount of LpxC in *yciM* deletion mutants has no change with or without FtsH, suggesting that YciM may act as an adaptor (Mahalakshmi et al., 2014). Besides, YciM can only regulate LpxC among all FtsH substrates indicating that YciM just affects the activity of FtsH specifically (Thomanek et al., 2018). In addition, YciS and YciM are reported to participate in LPS biogenesis together, because they were co-purified with LPS, FtsH, and Lpt proteins (Klein et al., 2014). The genes *yciS* and *yciM* belong to the RpoH regulon and their transcriptions were increased at 42°C, confirming that YciS and YciM are heat shock proteins. Recently, membrane protein YejM has been found to be closely related to LPS biogenesis regulation, in contrast to previous claims that its functions as a cardiolipin transporter (Clairfeuille et al., 2020). The suppressors that restored OM integrity caused by *yejM* deletion identified the *yciM*, *lpxC*, and *ftsH* gene, confirming that YejM is involved in LPS regulation (Fivenson and Bernhardt, 2020). YejM could bind LPS within the periplasmic leaflet of the inner membrane; the absence of YejM periplasm domain would cause LPS levels to increase and cells to be more sensitive to antibiotics. It is likely that YejM acts as an LPS monitor and coordinates with YciS, YciM, and FtsH to regulate LpxC levels. (Cian et al., 2019; Nguyen et al., 2020).

YciM is an inner membrane protein with one N-terminal transmembrane domain. It contains 389 amino acid residues and the crystal structure of YciM from *E. coli* comprises nine tetratricopeptide repeat (TPR) motifs and a C-terminal domain containing two Cys-x-x-Cys motifs (Prince and Jia, 2015). Interestingly, these Cys-x-x-Cys motifs are proposed to constitute a metal-binding site (Prince and Jia, 2015). However, the mechanism of YciM regulation of LPS biosynthesis and transport remains unknown.

In this study, we have determined the structure of the YciM cytoplasmic domain of *S. typhimurium* at 2.7 Å by X-ray crystallography. Our *in vitro* binding assays by isothermal titration calorimetry (ITC) showed that YciM could bind LPS and 3-hydroxtymyristic acid with affinity in the micromolar range, and it has a higher binding affinity to LPS than to 3-hydroxtymyristic acid. Our *in vitro* functional assays confirmed the importance of the lipid-binding residues. Furthermore, we demonstrated that YciM and YciS form a complex to regulate LPS biosynthesis and transport. Our study not only contributes to understanding the regulative mechanism of LPS biogenesis but also might help future anti-gram-negative bacteria drug discovery.

RESULTS

The overall structure of YciM from *S. typhimurium*

YciM of *S. typhimurium* was overexpressed and crystallized using an *in situ* limited proteolysis method with thermolysin at 1:1000 mass ratio (proteinase: protein). The resulting crystals belonged to space group $P2_122_1$ with cell dimensions a = 72.08 Å, b = 78.96 Å, c = 124.03 Å, and α = 90°, β = 90°, γ = 90° (Table S1). The structure was determined to a resolution of 2.7 Å by molecular replacement with one protomer of 4ZLH as a searching model. Crystal data collection and refinement statistics are listed in Table S1. There are two copies of YciM per asymmetric unit with a dimension of about 81.6 Å in length and 79.7 Å in height (Figure 1A). This structure contains 254 residues, from residue Glu136 to Gln389 with the final R_{factor} of 0.2480 and final R_{free} of 0.2489. The YciM soluble protein can be divided into two domains; the N-terminal domain and the C-terminal domain which form a bird wing shape with dimensions of approximately 36.4 Å in length and 79.7 Å in height. The N-terminal domain contains six TPR motifs while the C-terminal domain is the rubredoxin-like domain. The structures of the two protomers are almost identical with a root-mean-square deviation (RMSD) of 1.56 Å over 254 aligned residues, with some conformational changes at the TPR3, TPR4, and TPR8 motifs.

Lipid binding site

Dimeric YciM is formed through interactions of TPR7 and TPR8 of the protomers with an interface area of 1002.9 $Å^2$. Following refinement, extra electron density was observed at the interface between the protomers of the dimer to which we successfully docked an ethylene glycol. The F_O-F_C and $2F_O$-F_C map, which are respectively generated from refinement results without and with the ethylene glycol, are displayed in Figure S1. Hydrophobic residues L309, P313, M315, F318, M344, and V345 of both protomers create a hydrophobic tunnel that is responsible for the lipid binding, while residues T306, Q310, and Q348 may also interact with the lipid on the surface of the tunnel (Figures 1B and 1C). Conservation analysis showed that residues L309, P313, F318, L321, M322, and V345 are highly conserved, indicating these residues may play important roles in YciM functionality (Figure S2).

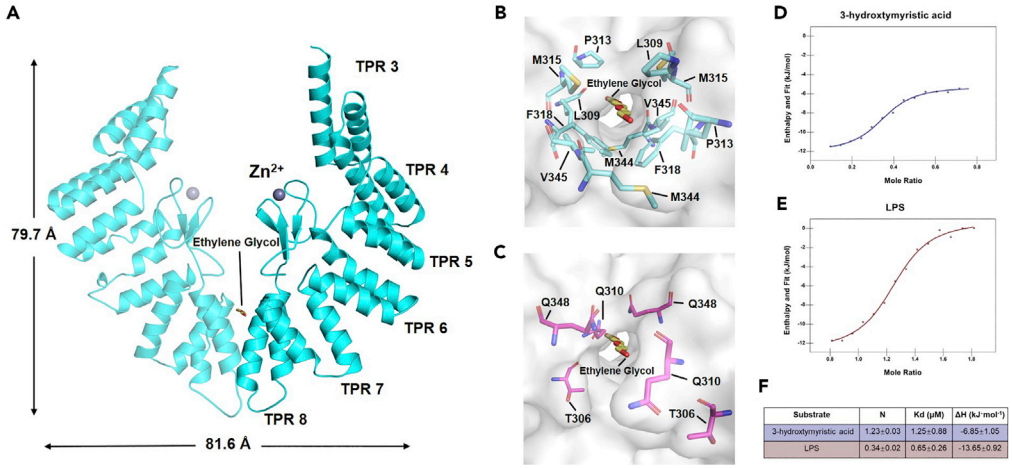

Substrate	N	Kd (μM)	ΔH (kJ·mol⁻¹)
3-hydroxtymyristic acid	1.23±0.03	1.25±0.88	-6.85±1.05
LPS	0.34±0.02	0.65±0.26	-13.65±0.92

Figure 1. Structure and affinity of *S. typhimurium* YciM lipid binding tunnel

(A) The structure of *S. typhimurium* YciM with ethylene glycol in its lipid binding tunnel. Two copies of YciM per asymmetric unit with dimensions of about 81.6 Å in length and 79.7 Å in height. The N-terminal domain of YciM contains six TPR motifs while the C-terminal contains two Cys-x-x-Cys motifs that locked a Zn^{2+} in site. The structure was displayed by PyMOL.

(B) Hydrophobic residues L309, P313, M315, F318, M344, and V345 of both protomers around the ethylene glycol create a hydrophobic tunnel that is responsible for the lipid binding. All residues were colored in cyan and the ethylene glycol was colored in yellow.

(C) Residues T306, Q310, and Q348 may interact with the lipid on the surface of the tunnel and were colored in magenta.

(D) Best fit single-site model of ITC thermogram resulting from titrating YciM soluble protein (0.067 mM, 1.4 mL, 20 mM TBS buffer, 1% DMSO, pH 8.0) and 3-hydroxtymyristic acid solution (0.3 mM, 250 μL, 20 mM TBS buffer, 1% DMSO, 4 μL injections). The titration was repeated three times. The ΔH and Kd of this exothermic interaction are −6.85 ± 1.05 $kJ \cdot mol^{-1}$ and 1.25 ± 0.88 μM, separately, demonstrating it is a favorable binding affinity.

(E) Best fit single-site model of ITC thermogram resulting from titrating YciM soluble protein (0.067 mM, 1.4 mL, 20 mM TBS buffer, pH 8.0) and LPS solution (0.3 mM, 250 μL, 20 mM TBS buffer, 4 μL injections). The titration was repeated three times. The ΔH and Kd of this exothermic interaction are −13.65 ± 0.92 $kJ \cdot mol^{-1}$ and 0.65 ± 0.26 μM, separately.

(F) The ITC measurement data of 3-hydroxtymyristic acid and LPS with protein YciM.

YciM prefers to bind LPS

According to the structural findings, we proposed that the hydrophobic tunnel of YciM might bind lipid molecules, like LPS intermediates. To test this hypothesis, YciM soluble domain's binding affinities to 3-hydroxymyristic acid and LPS were determined by ITC, which revealed that 3-hydroxtymyristic acid's Kd is 1.25 ± 0.88 μM and LPS's Kd is 0.65 ± 0.25 μM, suggesting that YciM binds lipids selectively and prefers to LPS. (Figures 1D and 1E) We also tested the calorimetric reaction between ethylene glycol and YciM (Figure S3). The calorimetric results indicate that the thermal effect of titration is mainly derived from the heat of dilution rather than the reaction, which also confirms that the conformational changes of lipid binding tunnel are caused by the entry of lipid molecules rather than crystallization solution.

Different conformations of YciM from *E. coli* and *S. typhimurium*

We compared our structure with the *E. coli* YciM (PDB code: 4ZLH) to figure out if there are different conformations of YciM. Our structure contains 254 residues, from residue Glu136 to Gln389 (Figure 2A), and the previously determined structure of the soluble domain of *E. coli* YciM consists of residues from G67 to L389 (Figure 2B) (Prince and Jia, 2015). The structure of a single copy of YciM from *S. typhimurium* reported here is very similar to that from *E. coli*, with an RMSD of 1.12 Å over 249 aligned residues (Figures 2E and 2F). However, superimposition of one protomer of the dimeric YciM from *E. coli* with that of dimeric YciM from *S. typhimurium* showed that the second protomer of the *E. coli* protein is rotationally shifted by approximately 40° and 31.9 Å at the widest point compared to that from *S. typhimurium* (Figures 2I and 2J).

Importantly, the lipid binding tunnel present in *S. typhimurium* YciM is closed by the TPR8 motif in *E. coli* YciM, consistent with the disappearance of the tunnel in the *E. coli* YciM structure (Figures 2C and 2D). The tunnel of *S. typhimurium* YciM was analyzed by HOLE (Smart et al., 1993), and we displayed the cavity

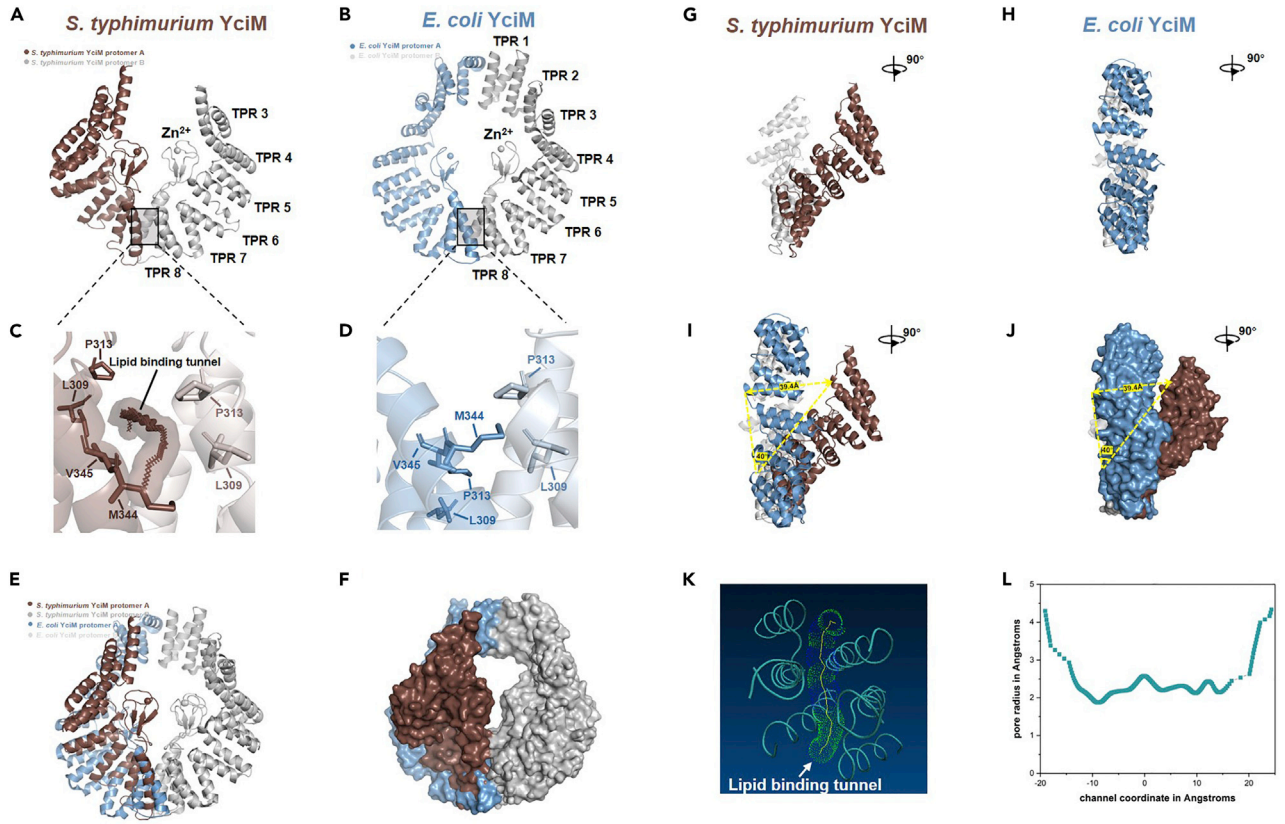

Figure 2. Superimposition of YciM between *S. typhimurium* and *E. coli*

(A) The structure of *S. typhimurium* YciM with six TPR motifs, while *E. coli* YciM (PDB code: 4ZLH) contains eight.

(B) Two TPRs of *S. typhimurium* YciM were cleaved during proteolysis crystallization. The protomer A of *E. coli* YciM and *S. typhimurium* YciM were colored in coffee and blue separately. The structure was displayed by PyMOL.

(C) The lipid binding tunnel of *S. typhimurium* YciM with an ethylene glycol inside which did not show in *E. coli* YciM.

(D) Hydrophobic residues L309, P313, M344, and V345 on the surface of lipid binding tunnel were indicated.

(E and F) (E) The superimposition of one protomer of YciM in *S. typhimurium* and *E. coli* at an RMSD of 1.12 Å over 249 aligned residues. The conformational difference can be found in the second protomer of YciM. The surface of the superimposition was shown in (F).

(G and H) Side view of *S. typhimurium* YciM and *E. coli* YciM after rotating 90° counterclockwise from the front view of dimer YciM.

(I and J) (I) Side view of *E. coli* YciM and *S. typhimurium* YciM superimposition. The view was rotated 90° counterclockwise from the front view of dimer YciM. It shows that the second protomer of the dimeric YciM from *E. coli* is rotationally shifted for about 40° and 39.4 Å at the widest point compared to that from *S. typhimurium*, which could be caused by conformational changes of YciM. The surface of the superimposition was shown in (J).

(K) Visualization of the cavity running through the lipid binding tunnel of *S. typhimurium* YciM by HOLE and VMD. The dots show the locus of the outer surface of a flexible sphere squeezing through the pore. The centerline of the pore is shown in yellow.

(L) The pore radius of the lipid binding tunnel changes with the channel coordinate. The pore radius within the *S. typhimurium* YciM tunnel varies between 1.8 and 2.4 Å.

running through the lipid binding tunnel of *S. typhimurium* YciM by VMD (Humphrey et al., 1996). The dots show the locus of the outer surface of a flexible sphere squeezing through the pore, and the lipid binding tunnel exists between two protomers of *S. typhimurium* YciM (Figure 2K). The radius is around 2 Å which appears in the middle of the tunnel (depths of 10 Å) (Figure 2L). The largest binding of lipid at the interface of the *S. typhimurium* YciM dimer may contribute to the observed rotational twist of the protomers compared to the *E. coli* YciM protein.

Lipid-binding residues are critical for bacterial growth

To study whether the tunnel residues involved in lipid binding are important for the function of YciM, a series of site-direct mutants (M315A/F318A/F318D/V345A/ V345D/Q348A/L386A) were generated by the site-direct-mutagenesis and *yciM* deletion strain was generated using the pEcCas/pEcgRNA system. The functional assays were performed in the Δ*yciM* strain (Figures 3A and 3B). Notably, we found that

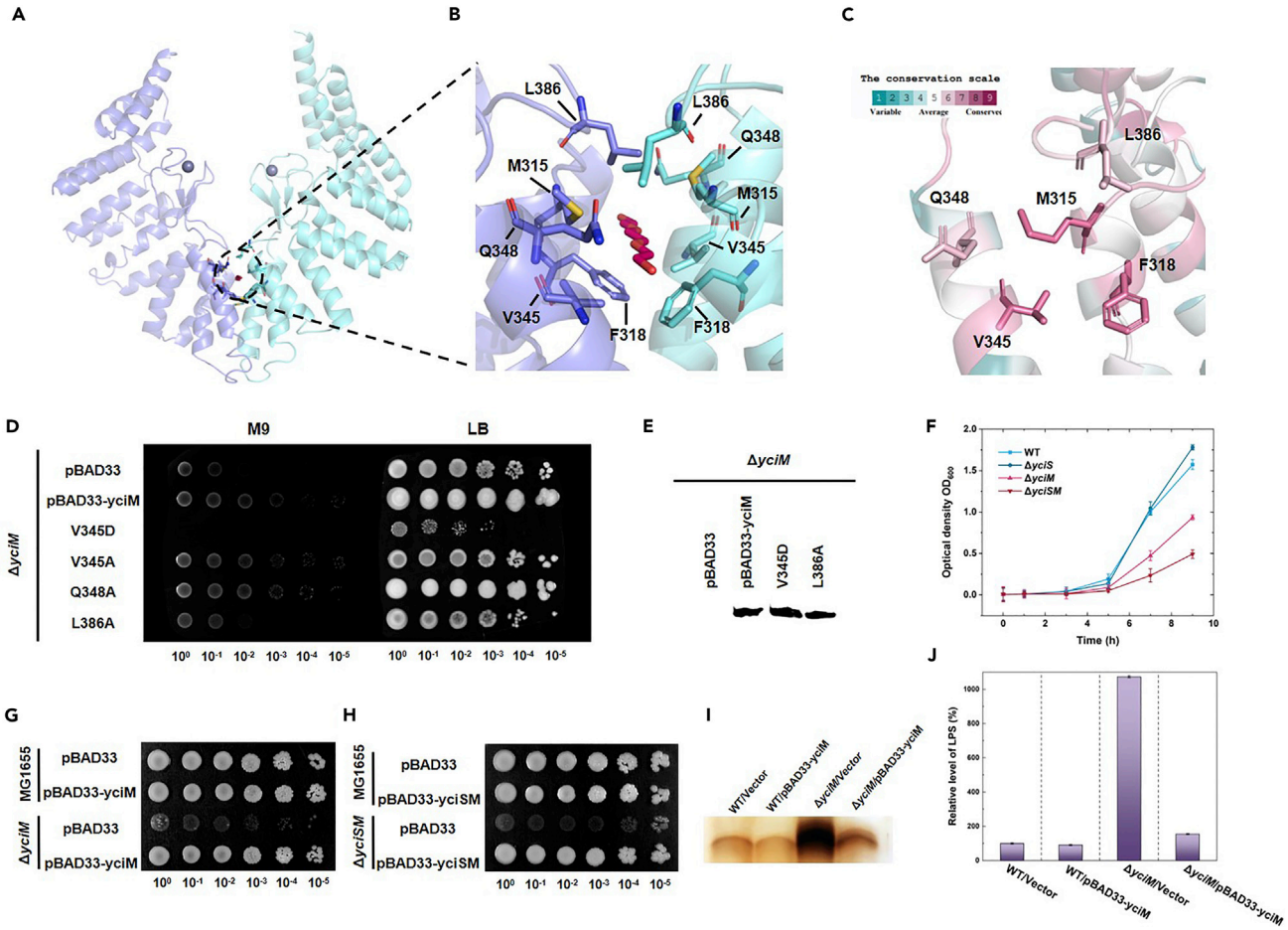

Figure 3. YciM is important for the growth and viability of *E.coli* and affects LPS biogenesis directly

(A and B) (A) Amino acid residues in the tunnel that could interact with lipid molecules, including M315, F318, V345, Q348, and L386. The surface map of these mutated amino acids was shown in (B). The structure was displayed in PyMOL.

(C) Surface map of mutated amino acids conservation in *S. typhimurium* YciM. The deep red of M315, F318, and V345 suggests they are highly conservative. The light pink of Q348 and L386 indicates their relatively high conservation.

(D) A series of site-directed mutants (M315A/F318A/F318D/V345A/V345D/Q348A/L386A) in knockout strain Δ*yciM* were generated to explore the function of the lipid binding tunnel of YciM. All strains were grown overnight in LB liquid medium supplemented with chloromycetin and 0.2% L-arabinose. Cells were harvested at 3, 000 × g for 5 min and washed by sterilized double distilled H_2O twice. The re-suspended culture was diluted to OD_{600} 1.0 and serially diluted at various dilutions (10^{-1}, 10^{-2}, 10^{-3}, 10^{-4}, 10^{-5}). 2 μL from each dilution were spotted on LB or M9 plates. Growth was scored after 48 h at 28°C. The functional assay was repeated in triplicate at least. Using PMB-103 (Δ*yciM* carrying an empty vector pBAD33) as the negative control, PMB-104 (Δ*yciM* carrying a plasmid pBAD33-yciM) as the positive control, the single mutant V345D and L386A caused grown defect in both LB and M9 plates, indicating the importance of lipid binding tunnel of YciM for bacteria survive.

(E) The expression level of mutants. The Western blot showed that the mutant protein expression levels are similar to that of the wild type.

(F) Growth curve of WT (MG1655), strain Δ*yciS*, Δ*yciM*, and Δ*yciSM*. All strains were cultured overnight in LB liquid medium at 37°C. Cells were harvested at 3, 000 × g for 5 min and washed by sterilized double distilled H_2O twice. The re-suspended culture was diluted at 1:100 ratio into M9 liquid medium and grown at 37°C. Growth was monitored by measuring OD_{600} every 1 h for 9 h. The assay was repeated in triplicate at least. The growth speed of strain Δ*yciS* was slightly lower than that of WT, but the growth speed of strain Δ*yciM* was far lower than that of both WT and stain Δ*yciS*, indicating that deleting *yciM* harmed the growth of *E. coli*. Notably, strain Δ*yciSM* grew worst among them, which suggests *yciS* cooperated with *yciM* in bacterial survival.

(G and H) (G) and (H) displayed the growth condition of strain Δ*yciM* and Δ*yciSM*, respectively. The culture condition and experimental procedure were as same as that of the site-directed mutant and used LB plate as the indicated plate. The functional assay was repeated in triplicate at least. PMB-101 (MG1655 carrying an empty vector pBAD33) is the control in this functional assay. PMB-103 and PMB-107 (Δ*yciSM* carrying an empty vector pBAD33) showed severe growth defects after cultivating at 28°C for about 48 h. But those defects were made up of *yciM* and *yciSM* complemental strains (PMB-104 and PMB-108). The growth condition of PMB-103 and PMB-107 is similar, meaning *yciM* is more crucial than yciS in the regulation process.

Figure 3. *Continued*

(I) Silver-stained tricine-SDS-PAGE gel shows LPS level in MG1655 or strain Δ*yciM* carrying pBAD33 or pBAD33-yciM. Strains were grown in presence of 0.2% L-arabinose to induce the expression of YciM. 16.5% SDS-Tricine gel was applied in this experiment, followed by silver staining to reveal LPS. The LPS extraction and measurement were repeated in triplicate at least.

(J) The relative level of LPS was measured by Image J. Using PMB-101 as control and defining its level of LPS as 100%. The relative LPS level of PMB-102 is 91.8 ± 3.3% of that of the control group. The LPS level of strain deleting *yciM* (PMB-103) increased 10.7 ± 0.06 folds based on PMB-101, suggesting that *yciM* deletion caused an urgent LPS accumulation. The LPS level of complemental strain is 1.54 ± 0.03 folds of that of PMB-101.

mutant V345D grew very poor in both LB and M9 plates. Mutant L386A also has grown defect in M9 plates, but it is not significant in LB plates (Figure 3D). We also checked the expression level of mutant V345D and L386A. The Western blot showed that the mutant protein expression levels are similar to that of the wild type (Figure 3E). To find out whether residue V345 is critical for the interaction between YciM and lipid molecules, we used ITC to test mutant V345D's binding affinities to 3-hydroxymyristic acid and LPS. Results reveal that mutant V345D could barely bind 3-hydroxymyristic acid or LPS (Figure S4). The negatively charged side chain of aspartic acid might disrupt the interaction between YciM and lipid molecules. Besides, L386 may play an important role through the hydrophobic interactions with lipids and the alanine mutation could abolish the interaction. It is worth noting that the conserved residue analysis using Consurf (Glaser et al., 2003) revealed that M315, F318, V345, Q348, and L386 are highly conservative (Figure 3C), indicating that our findings might be applied to YciM homologs in other strains.

YciS can be copurified with YciM

To validate the interaction between YciS and YciM in *S. typhimurium*, we generated constructs to overexpress YciM and YciS. When 8 × His tag was attached to the N-terminal of YciS, we found that it can be copurified with YciM (Figure S5A). Besides, YciS and YciM were also found together in fractions, even the 8 × His tag was changed to N-terminal of YciM (Figure S6). Meanwhile, we noticed that the band of YciS on SDS-PAGE was mainly smear-like, which was different from the result Klein G et al. found in *E. coli* (Klein et al., 2014). It spanned from 17 kDa to approximately 27 kDa (Figure S5B). To figure out whether the smear was caused by the non-specific binding of Ni column, we changed the N-terminal 8 × His tag of YciS to the Strep tag (tag sequence WSHPQFEK). Interestingly, we also found the smear band of YciS on SDS-PAGE, indicating that smear is the characteristic of YciS (Figure S7).

YciM and YciS are critical for growth and viability of *E.coli K12*

From the growth curve, Δ*yciM* strain grew very poor on M9 liquid medium at 37°C (Figure 3F). However, the Δ*yciS* strain only grew slightly slower than that of the wild type. The strain Δ*yciSM*, containing the deletion of both *yciS* and *yciM*, grew worse than strain Δ*yciM*, suggesting that *yciS* may cooperate with *yciM* in the survival of *E. coli*. All strains grew very well on LB medium means *yciM* is critical for *E. coli* when they are living in restrictive conditions, such as M9 medium. To further examine these observations, we constructed strain PMB-104 (Δ*yciM* carrying a plasmid pBAD33-yciM) and PMB-108 (Δ*yciSM* carrying a plasmid pBAD33-yciSM). The plasmid pBAD33 is unique in that the replication of the plasmid itself is dependent on the presence of L-arabinose. Deleting *yciM* or deleting both *yciS* and *yciM* caused *E. coli* to grow extremely sick on LB plates. However, overexpressing *yciM* or both *yciS* and *yciM* has no effect on the growth of *E. coli* (Figures 4G and 4H) Together, these results showed that the *yciM* gene is important for *E. coli* to survive.

yciM negatively regulates LPS level

To figure out why the deletion of *yciM* caused cell death, we measured the amount of LPS using Tricine-SDS-PAGE and silver staining (Figure 3I). Our result showed that the level of LPS is much higher in *yciM* deletion strain (at least ten times) compared with that of the parental strain (Figures 3I and 3J), which is consistent with the previous report (Mahalakshmi et al., 2014). Besides, the amount of LPS of stain PMB-102 (MG1655 carrying a plasmid pBAD33-yciM and in the presence of 0.2% L-arabinose) was slightly lower than that of wild type, indicating that overexpressed YciM leads to a decrease in LPS level. Meanwhile, the complemental strain PMB-104 with additional copies of *yciM* produced a higher amount of LPS than the wild type, but still far lower than that produced by strain PMB-103 (Δ*yciM* carrying an empty vector pBAD33).

DISCUSSION

In this study, we sought to better understand the role of the membrane proteins YciS and YciM in LPS biogenesis. Structurally, YciM contains a TPR domain mediating protein-protein interactions and a

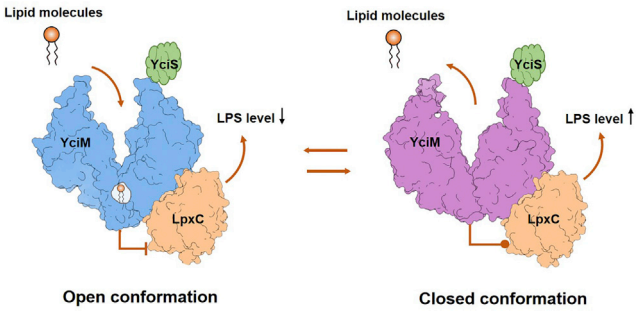

Figure 4. Two different conformations of YciM affect LPS level

The open conformation of YciM allows lipid molecules to bind the lipid binding tunnel. When YciM was activated, it would deliver LpxC to FtsH and LpxC's activity was inhibited, thus causing the LPS level to decrease. After lipid molecules leaves, YciM returns to its closed conformation and combines with YejM, followed by LpxC was activated to produce LPS.

zinc-binding domain with four cysteine residues locking a zinc ion in site. Based on the two YciM structures, we anticipate that YciM serves as a "switcher", which could bind and release a lipid substrate by changing conformation when anchored in the IM inner leaflet. Residues V345 and L386 in the lipid binding tunnel are highly conserved and play important roles in the functionality of YciM. Their interactions with potential substrates are essential for cell survival. Our ITC results showed that LPS and 3-hydroxtymyristic acid appear to bind YciM's soluble domain compared to the control molecule ethylene glycol which is accidentally observed in the crystal structure. Due to the micromolar affinity of the YciM soluble portion to LPS and LPS precursors, the threshold of LPS fully occupying the potential binding site could be quite high, and other lipid molecules, such as phospholipids, also have a great chance to bind to the site. Furthermore, the cellular environment is much more complicated, and the transmembrane domain of YciM could anchor YciM into the membrane and all the lipids inside the membrane could compete this binding site. Considering the competition of lipid from the inner membrane, the Kd of YciM to other lipid molecules should be measured by several advanced techniques in the future to further investigate this. After mutating residue V345 in the lipid binding tunnel, YciM lost the ability of binding lipid molecules, like 3-hydroxtymyristic acid or even LPS. Those results enhance our proposed "switcher" functionality of YciM. During the pull-down experiment, YciS could be co-purified with YciM which provided important clues concerning their function in mediating LPS regulation. Mutants absenting *yciS* and *yciM* have poorer growth than that absenting *yciM* suggested YciS could coordinate with YciM in regulating LPS biogenesis. An extremely high level of LPS in *yciM* deletion mutants leads to cell death, which was matched with results observed by Klein G et al. (Klein et al., 2014). According to previous studies by Fuhrer F et al. (Fuhrer et al., 2007), FtsH cooperates with YciM in the degradation of LpxC. Therefore, in the absence of YciM, LpxC would not be degraded and caused an urgent accumulation of LPS. Besides, overexpressing YciM would lead to over degradation of LpxC and the level of LPS decreasing. Our data suggest that YciM is a finely controlled negative regulator of LPS.

Although the structure of YciM in *E. coli* has been identified by Prince et al., in 2015, the function of YciM has not been clarified, leaving the roles YciM played in LPS regulation unclear (Prince and Jia, 2015). FtsH and YciM have been proved to affect lipid A biogenesis directly (Fuhrer et al., 2007). IM protein YejM could interact with LPS regulation proteins (like YciM or FtsH) by its periplasmic domain (Cian et al., 2019; Clairfeuille et al., 2020). Based on the obtained results, we supposed an LPS regulation mechanism of YciS and YciM: when the level of LPS decrease, YejM would combine YciM to prevent the interaction between FtsH and LpxC, which allows LpxC to produce LPS; when the LPS level is too high in bacteria, the lipid binding tunnel could interact with lipid substrates and activate YciM, then LpxC would be delivered by YciM and degraded by protease FtsH to curb the lipid A synthesis. If the lipid binding tunnel of YciM loses its functionality, it could not combine lipid substrates and could not deliver LpxC to FtsH, which caused the LPS level to elevate. The open conformation allows YciM to bind lipid molecules and inhibit LpxC's activity, thus reducing the LPS level. After lipid molecules detaches from the lipid binding tunnel, YciM would return to closed conformation and active LpxC, which induces the production of LPS (Figure 4). YciS may play a role in stabilizing YciM in the regulation mechanism. When the balance between LPS and phospholipid of the membrane was broken, cell permeability would increase that making cells become more fragile and are hard to resist the intrusion of toxin substance.

In summary, our results suggest that YciM is important for cell growth and could act as a "switcher" to regulate the LPS level. It would be worthwhile to test this model and also examine the mechanistic aspects of LPS regulation by YciS/YciM.

Limitations of the study

This study promotes additional information for our understanding of the LPS regulation mechanism via YciS/YciM. But there are still some limitations. For instance, the lipid binding tunnel in YciM has affinity to several lipid molecules. There could be a possibility that YciM might even play multi-roles in other bacterial life events, but what kind of lipid molecules still needs to be explored. Furthermore, when YciM is anchored in the membrane, the binding competition from different kinds of lipid from the membrane compositions would occur; the affinity of YciM to other lipid molecules should be measured by several advanced techniques to further investigate this.

STAR★METHODS

Detailed methods are provided in the online version of this paper and include the following:

- KEY RESOURCES TABLE
- RESOURCE AVAILABILITY
  - Lead contact
  - Materials availability
  - Data and code availability
- EXPERIMENTAL MODEL AND SUBJECT DETAILS
  - Strains and culture condition
- METHOD DETAILS
  - Plasmid construction
  - Expression and purification of membrane protein complex YciS and YciM
  - Expression and purification of cytoplasmic domain of YciM
  - Crystallization of cytoplasmic domain of YciM
  - X-ray data collection and structure determination
  - Isothermal titration calorimetry (ITC)
  - Null mutant generation
  - Growth curve
  - Growth and viability assays
  - Quantification of LPS
  - Site-directed mutagenesis
- QUANTIFICATION AND STATISTICAL ANALYSIS

SUPPLEMENTAL INFORMATION

Supplemental information can be found online at https://doi.org/10.1016/j.isci.2022.104988.

ACKNOWLEDGMENTS

This work was supported by the National Key R&D Program of China (2021YFC2100600) and the National Natural Science Foundation of China (31800052). We thank Prof. Yuhui Sun at Wuhan University to provide us the tool plasmids used for genome editing. We thank the staffs from BL17U, BL18U, and BL19U1 at Shanghai Synchrotron Radiation Facility (SSRF, China) and staffs from I03 at Diamond Light Source (UK) for assistance during X-ray data collection.

AUTHOR CONTRIBUTIONS

L.Y. generated the *yciSM* deletion strains and performed mutagenesis assays; H.H., H.L., and Z.Z. generated constructs and determined *S. typhimurium* YciM crystal structure; X.L. performed protein and ligand binding affinity assays. L.Y. wrote the paper; Z.D. discussed and revised the paper; C.D. and Z.Z. conceived the study, analyzed the data, and wrote the paper.

DECLARATION OF INTERESTS

The authors declare no competing interests.

Received: March 31, 2022
Revised: June 4, 2022
Accepted: August 17, 2022
Published: September 16, 2022

REFERENCES

Adachi, H., Takano, K., Morikawa, M., Kanaya, S., Yoshimura, M., Mori, Y., and Sasaki, T. (2003). Application of a two-liquid system to sitting-drop vapour-diffusion protein crystallization. Acta Crystallogr. D Biol. Crystallogr. *59*, 194–196. https://doi.org/10.1107/s0907444902019741.

Barb, A.W., and Zhou, P. (2008). Mechanism and inhibition of LpxC: an essential zinc-dependent deacetylase of bacterial lipid A synthesis. Curr. Pharm. Biotechnol. *9*, 9–15. https://doi.org/10.2174/138920108783497668.

Barb, A.W., Jiang, L., Raetz, C.R.H., and Zhou, P. (2007). Structure of the deacetylase LpxC bound to the antibiotic CHIR-090: time-dependent inhibition and specificity in ligand binding. Proc. Natl. Acad. Sci. USA *104*, 18433–18438. https://doi.org/10.1073/pnas.0709412104.

Cha, J.S., Pujol, C., and Kado, C.I. (1997). Identification and characterization of a Pantoea citrea gene encoding glucose dehydrogenase that is essential for causing pink disease of pineapple. Appl. Environ. Microbiol. *63*, 71–76. https://doi.org/10.1128/aem.63.1.71-76.1997.

Cian, M.B., Giordano, N.P., Masilamani, R., Minor, K.E., and Dalebroux, Z.D. (2019). Salmonella enterica serovar typhimurium uses PbgA/YejM to regulate lipopolysaccharide assembly during bacteremia. Infect. Immun. *88*. e00758-19. https://doi.org/10.1128/IAI.00758-19.

Clairfeuille, T., Buchholz, K.R., Li, Q., Verschueren, E., Liu, P., Sangaraju, D., Park, S., Noland, C.L., Storek, K.M., Nickerson, N.N., et al. (2020). Structure of the essential inner membrane lipopolysaccharide-PbgA complex. Nature *584*, 479–483. https://doi.org/10.1038/s41586-020-2597-x.

Collaborative Computational Project Number 4 (1994). The CCP4 suite: programs for protein crystallography. Acta Crystallogr. D Biol. Crystallogr. *50*, 760–763. https://doi.org/10.1107/S0907444994003112.

Davis Jr, M.R., and Goldberg, J.B. (2012). Purification and visualization of lipopolysaccharide from Gram-negative bacteria by hot aqueous-phenol extraction. J. Vis. Exp. *10*, 3916.

Emiola, A., Andrews, S.S., Heller, C., and George, J. (2016). Crosstalk between the lipopolysaccharide and phospholipid pathways during outer membrane biogenesis in *Escherichia coli*. Proc. Natl. Acad. Sci. USA *113*, 3108–3113. https://doi.org/10.1073/pnas.1521168113.

Fivenson, E.M., and Bernhardt, T.G. (2020). An essential membrane protein modulates the proteolysis of LpxC to control lipopolysaccharide synthesis in *Escherichia coli*. mBio *11*. e00939-20. https://doi.org/10.1128/mBio.00939-20.

Führer, F., Müller, A., Baumann, H., Langklotz, S., Kutscher, B., and Narberhaus, F. (2007). Sequence and length recognition of the C-terminal turnover element of LpxC, a soluble substrate of the membrane-bound FtsH protease. J. Mol. Biol. *372*, 485–496. https://doi.org/10.1016/j.jmb.2007.06.083.

Glaser, F., Pupko, T., Paz, I., Bell, R.E., Bechor-Shental, D., Martz, E., and Ben-Tal, N. (2003). ConSurf: identification of functional regions in proteins by surface-mapping of phylogenetic information. Bioinformatics *19*, 163–164. https://doi.org/10.1093/bioinformatics/19.1.163.

Heath, R.J., and Rock, C.O. (1996). Roles of the FabA and FabZ beta-hydroxyacyl-acyl carrier protein dehydratases in Escherichia coli fatty acid biosynthesis. J. Biol. Chem. *271*, 27795–27801.

Henderson, J.C., Zimmerman, S.M., Crofts, A.A., Boll, J.M., Kuhns, L.G., Herrera, C.M., and Trent, M.S. (2016). The power of asymmetry: architecture and assembly of the gram-negative outer membrane lipid bilayer. Annu. Rev. Microbiol. *70*, 255–278. https://doi.org/10.1146/annurev-micro-102215-095308.

Humphrey, W., Dalke, A., and Schulten, K. (1996). VMD: visual molecular dynamics. J. Mol. Graph. *14*, 33–38. https://doi.org/10.1016/0263-7855(96)00018-5.

Jackman, J.E., Fierke, C.A., Tumey, L.N., Pirrung, M., Uchiyama, T., Tahir, S.H., Hindsgaul, O., and Raetz, C.R. (2000). Antibacterial agents that target lipid A biosynthesis in gram-negative bacteria. Inhibition of diverse UDP-3-O-(r-3-hydroxymyristoyl)-n-acetylglucosamine deacetylases by substrate analogs containing zinc binding motifs. J. Biol. Chem. *275*, 11002–11009. https://doi.org/10.1074/jbc.275.15.11002.

Kabsch, W. (2010). Xds. Acta Crystallogr. D Biol. Crystallogr. *66*, 125–132. https://doi.org/10.1107/S0907444909047337.

Klein, G., Kobylak, N., Lindner, B., Stupak, A., and Raina, S. (2014). Assembly of lipopolysaccharide in *Escherichia coli* requires the essential LapB heat shock protein. J. Biol. Chem. *289*, 14829–14853. https://doi.org/10.1074/jbc.M113.539494.

Klein, G., Lindner, B., Brade, H., and Raina, S. (2011). Molecular basis of lipopolysaccharide heterogeneity in Escherichia coli: envelope stress-responsive regulators control the incorporation of glycoforms with a third 3-deoxy-alpha-D-manno-oct-2-ulosonic acid and rhamnose. J. Biol. Chem. *286*, 42787–42807. https://doi.org/10.1074/jbc.M111.291799.

Konovalova, A., Kahne, D.E., and Silhavy, T.J. (2017). Outer membrane biogenesis. Annu. Rev. Microbiol. *71*, 539–556. https://doi.org/10.1146/annurev-micro-090816-093754.

Li, Q., Sun, B., Chen, J., Zhang, Y., Jiang, Y., and Yang, S. (2021). A modified pCas/pTargetF system for CRISPR-Cas9-assisted genome editing in Escherichia coli. Acta Biochim. Biophys. Sin. *53*, 620–627. https://doi.org/10.1093/abbs/gmab036.

Liebschner, D., Afonine, P.V., Baker, M.L., Bunkóczi, G., Chen, V.B., Croll, T.I., Hintze, B., Hung, L.W., Jain, S., McCoy, A.J., et al. (2019). Macromolecular structure determination using X-rays, neutrons and electrons: recent developments in Phenix. Acta Crystallogr. D Struct. Biol. *75*, 861–877. https://doi.org/10.1107/S2059798319011471.

Liu, H., and Naismith, J.H. (2008). An efficient one-step site-directed deletion, insertion, single and multiple-site plasmid mutagenesis protocol. BMC Biotechnol. *8*, 91. https://doi.org/10.1186/1472-6750-8-91.

Mahalakshmi, S., Sunayana, M.R., Saisree, L., and Reddy, M. (2014). yciM is an essential gene required for regulation of lipopolysaccharide synthesis in Escherichia coli. Mol. Microbiol. *91*, 145–157.

McCoy, A.J., Grosse-Kunstleve, R.W., Adams, P.D., Winn, M.D., Storoni, L.C., and Read, R.J. (2007). Phaser crystallographic software. J. Appl. Crystallogr. *40*, 658–674. https://doi.org/10.1107/S0021889807021206.

Moffatt, J.H., Harper, M., and Boyce, J.D. (2019). Mechanisms of polymyxin resistance. Adv. Exp. Med. Biol. *1145*, 55–71. https://doi.org/10.1007/978-3-030-16373-0_5.

Murshudov, G.N., Vagin, A.A., and Dodson, E.J. (1997). Refinement of macromolecular structures by the maximum-likelihood method. Acta Crystallogr. D Biol. Crystallogr. *53*, 240–255. https://doi.org/10.1107/S0907444996012255.

Nguyen, D., Kelly, K., Qiu, N., and Misra, R. (2020). YejM controls LpxC levels by regulating protease activity of the FtsH/YciM complex of Escherichia coli. J. Bacteriol. *202*. e00303-20. https://doi.org/10.1128/JB.00303-20.

Piizzi, G., Parker, D.T., Peng, Y., Dobler, M., Patnaik, A., Wattanasin, S., Liu, E., Lenoir, F., Nunez, J., Kerrigan, J., et al. (2017). Design, synthesis, and properties of a potent inhibitor of Pseudomonas aeruginosa deacetylase LpxC. J. Med. Chem. *60*, 5002–5014. https://doi.org/10.1021/acs.jmedchem.7b00377.

Prince, C., and Jia, Z. (2015). An unexpected duo: rubredoxin binds nine TPR motifs to form LapB, an essential regulator of lipopolysaccharide synthesis. Structure *23*, 1500–1506. https://doi.org/10.1016/j.str.2015.06.011.

Pujol, C.J., and Kado, C.I. (2000). Genetic and biochemical characterization of the pathway in Pantoea citrea leading to pink disease of pineapple. J. Bacteriol. *182*, 2230–2237. https://doi.org/10.1128/JB.182.8.2230-2237.2000.

Sharan, S.K., Thomason, L.C., Kuznetsov, S.G., and Court, D.L. (2009). Recombineering: a homologous recombination-based method of genetic engineering. Nat. Protoc. *4*, 206–223. https://doi.org/10.1038/nprot.2008.227.

Smart, O.S., Goodfellow, J.M., and Wallace, B.A. (1993). The pore dimensions of gramicidin A. Biophys. J. *65*, 2455–2460. https://doi.org/10.1016/S0006-3495(93)81293-1.

Strong, M., Sawaya, M.R., Wang, S., Phillips, M., Cascio, D., and Eisenberg, D. (2006). Toward the structural genomics of complexes: crystal structure of a PE/PPE protein complex from Mycobacterium tuberculosis. Proc. Natl. Acad. Sci. USA *103*, 8060–8065. https://doi.org/10.1073/pnas.0602606103.

Thomanek, N., Arends, J., Lindemann, C., Barkovits, K., Meyer, H.E., Marcus, K., and Narberhaus, F. (2018). Intricate crosstalk between lipopolysaccharide, phospholipid and fatty acid metabolism in *Escherichia coli* modulates proteolysis of LpxC. Front. Microbiol. *9*, 3285. https://doi.org/10.3389/fmicb.2018.03285.

Tomaras, A.P., McPherson, C.J., Kuhn, M., Carifa, A., Mullins, L., George, D., Desbonnet, C., Eidem, T.M., Montgomery, J.I., Brown, M.F., et al. (2014). LpxC inhibitors as new antibacterial agents and tools for studying regulation of lipid A biosynthesis in Gram-negative pathogens. mBio *5*. e01551-01514. https://doi.org/10.1128/mBio.01551-14.

Wang, X., and Quinn, P.J. (2010). Lipopolysaccharide: biosynthetic pathway and structure modification. Prog. Lipid Res. *49*, 97–107. https://doi.org/10.1016/j.plipres.2009.06.002.

Wang, X., Quinn, P.J., and Yan, A. (2015). Kdo2-lipid A: structural diversity and impact on immunopharmacology. Biol. Rev. Camb. Philos. Soc. *90*, 408–427. https://doi.org/10.1111/brv.12114.

Williams, A.H., and Raetz, C.R.H. (2007). Structural basis for the acyl chain selectivity and mechanism of UDP-N-acetylglucosamine acyltransferase. Proc. Natl. Acad. Sci. USA *104*, 13543–13550.

Wiseman, T., Williston, S., Brandts, J.F., and Lin, L.N. (1989). Rapid measurement of binding constants and heats of binding using a new titration calorimeter. Anal. Biochem. *179*, 131–137. https://doi.org/10.1016/0003-2697(89)90213-3.

Zhang, L., Xiao, J., Xu, J., Fu, T., Cao, Z., Zhu, L., Chen, H.Z., Shen, X., Jiang, H., and Zhang, L. (2016). Crystal structure of FabZ-ACP complex reveals a dynamic seesaw-like catalytic mechanism of dehydratase in fatty acid biosynthesis. Cell Res. *26*, 1330–1344. https://doi.org/10.1038/cr.2016.136.

STAR★METHODS

KEY RESOURCES TABLE

REAGENT or RESOURCE	SOURCE	IDENTIFIER
Antibodies		
Mouse Anti-Streptavidin epitope tag (Strep-Tag) Monoclonal Antibody, Unconjugated, Clone Strep-tag II	Sigma-Aldrich	RRID:AB_1007528
Goat Anti-Mouse Goat anti-mouse IgG-HRP Polyclonal, Hrp Conjugated	Sigma-Aldrich	RRID:AB_631736
Bacterial and virus strains		
Escherichia coli MG1655	ATCC	ATCC 700926
Salmonella enterica subsp. enterica serovar Typhimurium LT2	ATCC	ATCC 700720
ΔyciS	This study	N/A
ΔyciM	This study	N/A
ΔyciSM	This study	N/A
PMB-101 (MG1655::Chl/pBAD33)	This study	N/A
PMB-102 (MG1655::Chl/pBAD33-yciM)	This study	N/A
PMB-103 (ΔyciM::Chl/pBAD33)	This study	N/A
PMB-104 (ΔyciM::Chl/pBAD33-yciM)	This study	N/A
PMB-105 (ΔyciM::Chl/P_{wild}-yciM)	This study	N/A
PMB-106 (MG1655::Chl/pBAD33-yciSM)	This study	N/A
PMB-107 (ΔyciSM::Chl/pBAD33)	This study	N/A
PMB-108 (ΔyciSM::Chl/pBAD33-yciSM)	This study	N/A
Chemicals, peptides, and recombinant proteins		
SUMO-YciM	This study	N/A
YciS-YciM	This study	N/A
Experimental models: Organisms/strains		
Escherichia coli MG1655	ATCC	ATCC 700926
Recombinant DNA		
Plasmid: pET-28a(+)-YciS	This study	N/A
Plasmid: pET-28a(+)-YciM	This study	N/A
Plasmid: pET-28a(+)-YciSM	This study	N/A
Plasmid: pBAD33-yciM	This study	N/A
Plasmid: pBAD33-yciSM	This study	N/A
Software and algorithms		
XDSGUI	Kabsch (2010)	XDS Package (mpg.de)
Diffraction Anisotropy Server	Strong et al. (2006)	Services – UCLA-DOE Institute | Diffraction Anisotropy Server
Phaser-MR	McCoy et al. (2007)	https://phenix-online.org/
CCP4i	Liebschner et al. (2019)	CCP4i: The CCP4 Graphical User Interface
Refmac5	Murshudov et al. (1997)	CCP4i: The CCP4 Graphical User Interface
Pymol	De-Lano Scientific	PyMOL | pymol.org
Deposited data		
The structure of *S. typhimurium* YciM	This study	PDB code: 7WZB
The structure of *E. coli* YciM	Prince and Jia (2015)	PDB code: 4ZLH

RESOURCE AVAILABILITY

Lead contact

Further information and requests for resources and reagents should be directed to and will be fulfilled by the lead contact, Zhenyu Zhang (zhengyu.zhang@whu.edu.cn).

Materials availability

This study did not generate new unique reagents.

Data and code availability

- Data

The X-ray structures of *S. typhimurium* YciM was deposited in the Protein Data Bank under accession codes 7WZB. All other data generated and analyzed in this study are available within the article and the Supplementary Information.

- Code

This study did not generate any code.

- Additional information

Any additional information required to reanalyze the data reported in this paper is available from the lead contact upon reasonable request.

EXPERIMENTAL MODEL AND SUBJECT DETAILS

Strains and culture condition

E. coli MG 1655 was used as the experimental model for null mutant generation

Strains were cultured in Luria–Bertani (LB) medium (1% tryptone, 0.5% yeast extract, and 1% NaCl) or M9 Minimal medium (85.52 g/L $Na_2HPO_4 \cdot 12H_2O$, 15 g/L KH_2PO_4, 2.5 g/L NaCl, 5 g/L NH_4Cl) supplemented with appropriate antibiotics. The following antibiotics were used at the indicated concentrations: kanamycin (Kan), 50 μg/mL; spectinomycin (Spc), 50 μg/mL, chloromycetin (Chl), 25 μg/mL.

METHOD DETAILS

Plasmid construction

Two DNA fragments containing *yciS* and *yciM* were amplified from the genome DNA of wild-type strain *S. typhimurium* separately. The DNA fragments were purified with DNA gel extraction kit (Magen, China) and then cloned into pET-28a(+) vector to generate pET-28a(+)-yciS and pET-28a(+)-yciM respectively. *yciS* and *yciM* are consecutive genes on the genome of wild-type strain *S. typhimurium*. So DNA fragments containing *yciS* and *yciM* were amplified from *S. typhimurium* together to construct pET-28a(+)-yciSM, and the 8 × His tag was attached to the N-terminal of *yciS*.

Expression and purification of membrane protein complex YciS and YciM

The plasmid pET-28a(+)-yciSM was transformed into *E. coli* C43(DE3) cells to express proteins. A single colony was inoculated into 10 mL LB liquid medium supplemented with kanamycin and cultured at 37°C overnight. The overnight seed culture was inoculated (1:100) into LB liquid medium supplemented with kanamycin and grown at 37°C until the OD_{600} reached 0.8–1.0, then the proteins were induced by adding 0.1 mM isopropyl β-D-thiogalactoside (IPTG) for 14 h at 20°C with shaking at 220 rpm. Cells were harvested by centrifugation at 5,000 × g and re-suspended in TBS buffer (20 mM Tris-HCl, 300 mM NaCl, pH 8.0). The cell pellets were lysed by passing through a cell disruptor (ATS, China) at 30,000 psi. The unbroken cells and cell debris were removed by centrifugation at 10,000 × g for 1 h at 4°C. The supernatant was ultracentrifuged at 140,000 × g for 1h at 4°C, and the membrane pellet was solubilized with an extraction buffer (20 mM Tris-HCl, 300 mM NaCl, 20 mM imidazole,1% (w/v) n-Dodecyl-β-D-Maltopyranoside (DDM), pH 8.0) at 4°C for 1h. The supernatant was then centrifuged at 10,000 × g for 30 min before being loaded onto a 5 mL of HisTrap-HP column (GE Healthcare). The column was pre-equilibrated with a balance buffer (20 mM Tris-HCl, 300 mM NaCl, 20 mM imidazole, 0.05% DDM, pH 8.0) and washed by a wash buffer (20 mM Tris-HCl, 300 mM NaCl, 40 mM imidazole, 0.05% DDM, pH 8.0). The proteins were eluted by an elution buffer (20 mM Tris-HCl, 300 mM NaCl, 300 mM imidazole, 0.05% DDM, pH 8.0), and further purified

by the size exclusion chromatography with a Superdex 200 size-exclusion column (GE Healthcare). The purity of protein was checked using SDS-PAGE. All the purification processes were performed at 4 °C.

Expression and purification of cytoplasmic domain of YciM

The plasmid was transformed into *E. coli* BL21(DE3) cells to express proteins. Culture condition was as same as described previously. Cells were harvested by centrifugation at 5,000 × g and re-suspended in the lysis buffer (20 mM Tris-HCl, 300 mM NaCl, 10% glycerol, pH 8.0) added with complete EDTA-free Protease Inhibitor Cocktail Tablet, 50 μg/mL DNase I and 100 μg/mL lysozyme. The cell pellets were lysed by passing them through a cell disruptor (ATS, China) at 30,000 psi. The unbroken cells and cell debris were removed by centrifugation at 16,000 × g for 30 min at 4°C. The supernatant was loaded onto a 5 mL of HisTrap-HP column (GE Healthcare) pre-equilibrated with the balance buffer (20 mM Tris-HCl, 300 mM NaCl, 20 mM imidazole, 10% glycerol, pH 8.0), The protein was washed by the wash buffer (20 mM Tris-HCl, 300 mM NaCl, 40 mM imidazole, 10% glycerol, pH 8.0) and eluted by the elution buffer (20 mM Tris-HCl, 300 mM NaCl, 500 mM imidazole, 10% glycerol, pH 8.0). The protein sample was desalted using a pre-equilibrated desalting column (GE Healthcare) with the TBS buffer to remove the high concentration of imidazole. TEV protease was added to the desalted protein at a TEV to protein mass ratio 1:100 and incubated at 4°C overnight. The post-cleavage mixture was loaded onto the pre-equilibrated 5 mL HP HisTrap column (GE Healthcare) again and collected. Collected proteins were further purified by the size exclusion chromatography with a Superdex 200 size-exclusion column (GE Healthcare). The purity of protein was checked using SDS-PAGE. All the purification processes were performed at 4°C.

Crystallization of cytoplasmic domain of YciM

For crystallization, protein in the TBS buffer (20 mM Tris, 300 mM NaCl, pH 8.0) was concentrated to 10 mg/mL after being digested by thermolysin at 1:500 mass ratio at room temperature for 4 h. Crystallization conditions were primarily screened by the Mosquito robot (TTP Lab Tech) with 96-well plates using commercial solution kits from Hampton Research at protein to buffer 2:1, 1:1, and 1:2 ratios. Best diffraction crystals were grown from 0.5 μL of protein YciM with 0.5 μL of the reservoir solution, using the sitting drop crystallization protocol (Adachi et al., 2003). The native YciM crystal was grown at 20 °C in 21.25% Ethylene glycol and 15% glycerol over 2 weeks. Crystals were flash frozen in a stream of liquid nitrogen before data collection.

X-ray data collection and structure determination

The X-ray diffraction data were collected at Diamond Light Source beamline I02 (UK) and Shanghai Synchrotron Radiation Facility beamline BL19U1 (China). The data were subsequently indexed, integrated, and scaled by XDSGUI program suite (Kabsch, 2010). The data appeared to be slightly anisotropic and was then corrected using UCLA-DOE LAB — Diffraction Anisotropy Server XDS processed data (Strong et al., 2006). The anisotropic truncated resolutions were 2.4 Å 2.4 Å 2.9 Å along a*, b*, c* directions respectively. The initial phases were determined by molecular replacement using CCP4i suite PhaserMR program (Liebschner et al., 2019; McCoy et al., 2007) with one protomer of 4ZLH as the searching model.

The crystal structure of *S. typhimurium* YciM cytoplasmic domain was then built using Buccaneer CCP4i (Collaborative Computational Project, 1994)and refined using Refmac5 (Murshudov et al., 1997). The crystal structure in this study greatly differs from that of 4ZLH. Our dimer structures shifted at a 40 degrees angle against each other compared to 4ZLH, thus opening a tunnel of potential lipid binding ability. The Crystal structure of *S. typhimurium* YciM cytoplasmic domain was determined at a resolution of 2.7 Å, which belonged to $P2_122_1$ space group with the cell dimensions of a = 72.08 Å, b =78.96 Å, c = 124.03 Å, and $\alpha = 90°$, $\beta = 90°$, $\gamma = 90°$, and two molecules in one asymmetric unit. Structure representations were prepared with PyMOL (DeLano Scientific). The geometries of the final structure were evaluated by PHENIX (Collaborative Computational Project, 1994) and the resulting coordinates and structure factors have been deposited in the Protein Data Bank (PDB code: 7WZB).

Isothermal titration calorimetry (ITC)

Experiments were performed using the Nano-ITC (TA, USA) in the standard buffer conditions given above. In each titration 60–70 μM protein, in the cell, was titrated with 25 injections of 300 μM ligand. The volume of each injection was 10 μL. Injections were continued beyond saturation level to allow for the determination of heats of ligand dilution. The resulting data were fit to a single-site binding isotherm

(Wiseman et al., 1989), with an additional term for the heat of dilution, using the NanoAnalyze software supplied with the calorimeter. Estimated errors in thermodynamic quantities are generated automatically by the software. The variation between repeated experiments at 25°C is consistent with these error estimates.

Null mutant generation

Complete deletion of *yciS*, *yciM* and both of *yciS* and *yciM* were constructed by pEcCas/pEcgRNA system provided by Li Q lab (Li et al., 2021). Special N20 sequence of each gene was designed using Benchling and fused with BsuI-linearized pTargetF using Golden Gate Assembly to yield target pEcgRNA for *yciS* and *yciM*. The electroporation of competent cells of *E. coli* MG1655 carrying pEcCas was performed using protocol provided by Cha et al.(Cha et al., 1997; Pujol and Kado, 2000; Sharan et al., 2009). The culture medium was supplemented with a final concentration of 10 mM L-arabinose to induce the expression of λ-Red system. For genome editing, 100 μL of competent cells were mixed with 100 ng of pEcgRNA series plasmids and 400 ng of donor DNA, and the mixture was electroporated in a precooled 1 mm Gene Pulser cuvette (Bio-Rad, Hurcules, USA) at 1.8 kV. The electroporation mixture was immediately suspended in 1 mL of fresh LB medium. Cells were recovered by incubating at 37°C for 1 h before spreading on LB plates containing kanamycin and spectinomycin, and the plates were then incubated overnight at 37°C. Individual colonies were randomly picked and verified by colony-PCR and DNA sequencing. The pEcgRNA series plasmids of verified strains were eliminated by methods provided by Li Q lab (Li et al., 2021).

Growth curve

Cells of overnight cultures of bacteria grown in 3 mL LB liquid medium at 37°C were harvested at 3,000 × g for 5 min and washed by sterilized double distilled H_2O twice. The re-suspended culture was diluted at 1:100 ratio into M9 liquid medium (supplemented with 0.2% D-glucose as the carbon source) and grown at 37°C with shaking at 220 rpm. Growth was monitored by measuring OD_{600} every 1 h for 9 h.

Growth and viability assays

A single colony of each strain was inoculated into 3 mL LB liquid medium supplemented with 0.2% L-arabinose and grown at 37°C overnight with shaking at 220 rpm. Cells were harvested at 3,000 × g for 5 min and washed by sterilized double distilled H_2O twice. The re-suspended culture was diluted to OD_{600} 1.0, and then serially diluted at various dilutions (10^{-1}, 10^{-2}, 10^{-3}, 10^{-4}, 10^{-5}). 2 μL aliquots of each dilution were spotted on indicated plates and incubated at 28°C for 48 h.

Quantification of LPS

The extraction of LPS according to an improved hot aqueous-phenol method from Davis M.R lab (Davis and Goldberg, 2012). A single colony of each strain was inoculated into 10 mL M9 medium supplemented with 0.2% L-arabinose and 0.2% D-glucose and grown at 37°C with shaking at 220 rpm for 24 h. The culture was diluted to OD_{600} 0.5 with M9 medium followed by centrifugation at 10, 600 × g for 10 min. Diluting 2 × stock (100 mM Tris-HCl, pH 6.8, 24% w/v glycerol, 8% w/v SDS, 5% v/v 2-β-mercaptoethanol, 0.02% w/v bromophenol blue) 1:1 in sterile distilled H_2O to prepare the 1 × tricine sample stock. Pelleted bacteria were re-suspended with 200 μL 1 × tricine sample buffer and boiled for 10 min. Adding 50 μg of both DNase I and RNase to samples and incubating at 37°C for 30 min. Then adding 100 μg of the Proteinase K to samples and incubating at 59°C for 3 h. To each sample, adding 200 μL of ice-cold Tris-saturated phenol and vertexing each sample for approximately 5 to 10 s. Samples was incubated at 65°C for 15 min and vortexed occasionally. After incubating cool to room temperature, and then adding 1 mL of room-temperature diethyl ether to each sample and vertexing for 5 to 10 s. Centrifuging the samples at 13,300 × g for 30 min. Carefully remove the samples from the centrifuge and extract the bottom blue layer. LPS were revealed by 16.5% Tricine-SDS-PAGE and sliver staining according to the manufacturer's instructions.

Site-directed mutagenesis

The full length of *yciM* was amplified from MG1655 and cloned into vector pBAD33 to generate pBAD33-yciM. Plasmids of mutagenesis were constructed using pBAD33-yciM as the template with different primers listed in Table S1. All site-directed mutants were generated following Liu, H. and J.H. Naismith's protocol (Liu and Naismith, 2008). Plasmids were sequenced to verify the desired mutants. The resultant plasmids were transformed into the competent cells Δ*yciM* using electroporation for characterization observation.

QUANTIFICATION AND STATISTICAL ANALYSIS

For LPS extraction and growth curve assays, data were plotted using Origin 2021. Pooled data from N = 3 separate experiments and Standard Deviation (SD) are shown.

For ITC experiments, data were processed by NanoAnalyze software supplied with the calorimeter to fit to a single-site binding isotherm. Estimated errors in thermodynamic quantities were generated automatically by the software.